Tracing the Ventilation Pathways of the Deep North Pacific Ocean Using Lagrangian Particles and Eulerian Tracers

Syed, Hyder Ali; Primeau, F.W.; Deleersnijder, Eric; Heemink, Arnold W.

DOI
10.1175/JPO-D-16-0098.1

Publication date
2017

Document Version
Final published version

Published in
Journal of Physical Oceanography

Tracing the Ventilation Pathways of the Deep North Pacific Ocean Using Lagrangian Particles and Eulerian Tracers

SYED HYDER ALI MUTTAQI SHAH

Delft Institute of Applied Mathematics, Delft University of Technology, Delft, Netherlands, and Department of Mathematics, Sukkur Institute of Business Administration, Sukkur, Pakistan

FRANÇOIS W. PRIMEAU

Department of Earth System Science, University of California, Irvine, Irvine, California

ERIC DELEERSNIJDER

Institute of Mechanics, Materials and Civil Engineering, and Earth and Life Institute, Université Catholique de Louvain, Louvain-la-Neuve, Belgium, and Delft Institute of Applied Mathematics, Delft University of Technology, Delft, Netherlands

ARNOLD W. HEEMINK

Delft Institute of Applied Mathematics, Delft University of Technology, Delft, Netherlands

(Manuscript received 3 May 2016, in final form 15 March 2017)

ABSTRACT

Lagrangian forward and backward models are introduced into a coarse-grid ocean global circulation model to trace the ventilation routes of the deep North Pacific Ocean. The random walk aspect in the Lagrangian model is dictated by a rotated isopycnal diffusivity tensor in the circulation model, and the effect of diffusion is explicitly resolved by means of stochastic terms in the Lagrangian model. The analogy between the probability distribution of a Lagrangian model with Green's function of an Eulerian tracer transport equation is established. The estimated first- and last-passage time density of the deep North Pacific using both the Eulerian and the Lagrangian models ensured that the Lagrangian pathways and their ensemble statistics are consistent with the Eulerian tracer transport and its adjoint model. Moreover, the sample pathways of the ventilated mass fractions of the deep North Pacific particles to and from the ocean surface are studied.

1. Introduction

To understand how climate change signals are communicated to the global ocean it is essential to determine the pathways and rates of water mass ventilation. A natural approach is to trace ocean water masses as they are transported to and from the sea surface along advective–diffusive pathways. A considerable observational effort is directed at tracing water mass movements using floats (Furey et al. 2001) and transient chemical tracers (Fine 2011). However, tracing the movement of water masses directly poses a considerable observational challenge because of the vastness of the ocean and the long deep-water renewal time scales that can extend to thousands of years.

An alternative approach is to use a numerical ocean model to simulate the global circulation and then to trace the movement of water masses in the simulated ocean using either Lagrangian or Eulerian tracers. Studies that have adopted the Eulerian approach have generally ignored pathway information to focus instead on summary diagnostics such as the fraction of the water originating from various surface patches or the mean transit time from the surface (i.e., the age), both of which are readily obtained by computing appropriate moments of the Green's function for the model's advective–diffusive tracer transport equation (e.g., Haine and Hall 2002; Primeau 2005; Peacock and Maltrud 2006; Primeau and Holzer 2006; DeVries and Primeau 2011). Notable exceptions are the path-density

Corresponding author: Syed Hyder Ali Muttaqi Shah, muttaqi_shah@yahoo.com

DOI: 10.1175/JPO-D-16-0098.1

diagnostic studies of Holzer and Primeau (2006, 2008) in which some averaged pathway information was extracted from Eulerian tracers. The path-density diagnostic notwithstanding, pathway information has generally been obtained from models that have adopted a Lagrangian framework to compute particle trajectories (Fujio and Imasato 1991; Fujio et al. 1992; Böning and Cox 1988; Doos 1995). In these Lagrangian studies, particle trajectories were computed by interpolating the model's explicitly resolved velocity along particle pathways. The diffusive transport due to subgrid-scale processes was neglected. However, in coarse-grained ocean circulation models the redistribution of tracers by parameterized eddy diffusive fluxes is an important part of the transport and its neglect leads to substantial errors (Hall et al. 2004).

More recent studies have used high-resolution, eddy-permitting models to compute Lagrangian pathways (Getzlaff et al. 2006; Bower et al. 2009, 2011; Gary et al. 2011; Lozier et al. 2012). By explicitly resolving mesoscale eddies, the computed advective Lagrangian trajectories include the effect of mesoscale eddies, but they still neglect the effect of subgrid-scale processes that lead to diapycnal diffusion. While diapycnal diffusivities are generally much smaller than isopycnal diffusivities their contribution to transport can become significant on long time scales and cannot be neglected for pathways that connect the deep ocean to the surface. Furthermore, the extreme computational costs associated with running eddy-resolving models have limited the application of Lagrangian trajectory diagnostics to relatively short time scales and regional domains. To trace out global conveyor pathways, multicentury to millennial time-scale calculations are needed, and only coarse-grained models with parameterized eddy diffusive fluxes have acceptable computational costs. It is therefore critical to take into account the effect of diffusion in addition to advection in the application of Lagrangian diagnostics to global models.

In the present study, we combine Eulerian and Lagrangian diagnostics in a complementary way to study the ventilation of the deep North Pacific Ocean (DNP) where the oldest water masses reside. To ensure that our results are relevant to the real ocean, we use a circulation model that was constrained by transient tracer observations of chlorofluorocarbon (CFC-11) in addition to climatological temperature, salinity, and natural (prebomb) radiocarbon (DeVries and Primeau 2011; DeVries 2014). The model, which is described more fully in section 2c, parameterizes eddy mixing using a diffusive parameterization with a rotated isopycnal diffusivity tensor (Redi 1982; Solomon 1971). From the point of view of the application of Lagrangian methods to a global ocean model, a novel aspect of our study is that we include a random walk component to our Lagrangian particles that is designed to ensure consistency with the nonisotropic diffusivity tensor used in the Eulerian tracer transport equation.

This article is organized as follows: In section 2a the Kolmogorov forward and backward equations for modeling tracer transport are first discussed, and the Lagrangian random walk equations consistent with the advection–diffusion equation and its adjoint are modeled. The probability distributions for the time to transport the Lagrangian particles to and from the surface are discussed in section 2b. The global ocean circulation model used in this study is briefly described in section 2c, and the numerical setting used for the diagnostic presented in this work is demonstrated in section 2d. The diagnostics for the time scales of the deep North Pacific Ocean to and from the sea surface is presented for both the Eulerian and Lagrangian calculations in section 3a. In section 3b, the locations where the deep North Pacific particles make their last and first contact with the sea surface are discussed and the ventilation of the ocean's oldest water mass using an Eulerian tracer diagnostic to partition the water in the deep North Pacific Ocean according to the surface region where it was last exposed to the atmosphere as well as the region where it will first be reexposed to the atmosphere is presented. Furthermore, the typical ventilation pathways computed using the Lagrangian counterpart of Kolmogorov forward and backward equations are also constructed in section 3c. Concluding remarks are presented in section 4.

2. Theory and methods

In this section, we present the methods we use for computing Lagrangian particle trajectories.

a. Kolmogorov equations for modeling transport

In probability theory, the time evolution of the probability distribution of a diffusion process is described by the forward and backward Kolmogorov equations. As will be explained later, these equations are equivalent to the Eulerian formulation of the forward and adjoint tracer transport equations. For a detailed description of the Kolmogorov equations, the reader is referred to, among others, Jazwinski (1970) or Gardiner (1985).

1) KOLMOGOROV FORWARD EQUATION

The Kolmogorov forward equation describes the evolution of a probability distribution forward in time from some starting time s to a future time t with $t > s$. For

our application, we consider the probability distribution for the position of a Lagrangian particle.

If we denote by $G(t, \mathbf{x}; s, \mathbf{y})$ the probability distribution of finding a particle at time t at location $\mathbf{x}$, given that it was at location $\mathbf{y}$ at time s, with $s < t$, then this probability distribution can be expressed in terms of a solution of the Kolmogorov forward equation:

$$\frac{\partial G(t,\mathbf{x};s,\mathbf{y})}{\partial t} + \mathscr{L} G(t,\mathbf{x};s,\mathbf{y}) = 0,$$
$$G(t=s,\mathbf{x};s,\mathbf{y}) = \delta(\mathbf{x}-\mathbf{y}). \quad (1)$$

The differential operator $\mathscr{L}$ consists of advective terms (given by vector $\mathbf{a} = a_i$) as well as diffusion-related terms (given by the matrix $\mathbf{b} = b_{ij}$) and is defined as follows:

$$\mathscr{L}(\cdot) \equiv \frac{\partial}{\partial x_i} a_i(t,\mathbf{x})(\cdot) - \frac{\partial}{\partial x_i \partial x_j} b_{ij}(t,\mathbf{x})(\cdot). \quad (2)$$

The diffusivity tensor b_{ij} must be positive definite and can be expressed in terms of a displacement matrix $\boldsymbol{\sigma}$:

$$b_{ij} = \frac{1}{2}(\boldsymbol{\sigma}\boldsymbol{\sigma}^{\mathrm{T}})_{ij}. \quad (3)$$

Notice that the matrix $\boldsymbol{\sigma}$ is not uniquely determined by the symmetric matrix $\mathbf{b}$. However, any choice of $\boldsymbol{\sigma}$ that satisfies Eq. (3) is correct and will result in statistically identical diffusion processes.

The Kolmogorov forward equation (1) can be solved by using a Lagrangian random walk model. In this approach, Eq. (1) is replaced by an equivalent Îto stochastic differential equation for the position of an individual particle:

$$d\mathbf{X}(t) = \mathbf{a}(\mathbf{X},t)dt + \boldsymbol{\sigma}(\mathbf{X},t)\cdot d\mathbf{W}(t), \quad \mathbf{X}(t=s) = \mathbf{y}, \quad (4)$$

where the vector $d\mathbf{W}$ is called the Wiener increment. The components dW_i of $d\mathbf{W}$ are all independent, normally distributed, random variables with zero mean and variance proportional to dt. The vector $\mathbf{X}$ represents the position of the particles, and the increments $d\mathbf{X} = \mathbf{X}(t + dt) - \mathbf{X}(t)$ describe the displacements of Lagrangian particles according to the effect of a deterministic displacement called the drift $\mathbf{a}(\mathbf{X}, t)dt$ and a stochastic displacement $\boldsymbol{\sigma}(\mathbf{X}, t)\cdot d\mathbf{W}(t)$ that is due to the parameterized eddy diffusion. The solutions $\mathbf{X}(t)$ of the stochastic processes given by Eq. (4) provide random samples from the probability distribution $G(t, \mathbf{x}; s, \mathbf{y})$.

The Îto calculus is a mathematical approach for realizing a unique solution to a stochastic differential equation. Stratonovich is an alternative method that can also be used to derive stochastic particle models. However, after discretization of the stochastic differential equation with an appropriate numerical scheme, mathematical subtleties introduced by the stochastic calculus are irrelevant. For more details about the numerical treatment of stochastic differential equations, the reader is referred to Kloeden and Platen (1992).

2) KOLMOGOROV BACKWARD EQUATION

The Kolmogorov backward equation is the formal adjoint of the Kolmogorov forward equation:

$$\frac{\partial G(t,\mathbf{x};s,\mathbf{y})}{\partial s} + \mathscr{L}^{\dagger} G(t,\mathbf{x};s,\mathbf{y}) = 0,$$
$$G(t,\mathbf{x};s=t,\mathbf{y}) = \delta(\mathbf{x}-\mathbf{y}), \quad (5)$$

where the differential operator $\mathscr{L}^{\dagger}$ is the adjoint of $\mathscr{L}$, that is,

$$\mathscr{L}^{\dagger}(\cdot) \equiv a_i(s,\mathbf{y})\frac{\partial}{\partial y_i}(\cdot) + b_{ij}(s,\mathbf{y})\frac{\partial}{\partial y_i \partial y_j}(\cdot). \quad (6)$$

The Kolmogorov backward equation governs the evolution of $G(t, \mathbf{x}; s, \mathbf{y})$ with respect to s for $s < t$. Note that in the case of the Kolmogorov forward equation, the state $(s, \mathbf{y})$ is held fixed so that the solution of the forward equation describes a probability distribution for the location $\mathbf{x}$ of a particle at successive times for $t > s$. In contrast, for the case of the Kolmogorov backward equation, it is the state $(t, \mathbf{x})$ that is held fixed, while $G(t, \mathbf{x}; s, \mathbf{y})$ as function of the initial position $\mathbf{y}$ evolves backward in time for $s < t$.

In general, the solution to the Kolmogorov backward equation $G(t, \mathbf{x}; s, \mathbf{y})$ does not necessarily describe a probability distribution with respect to $\mathbf{y}$. However, we will show later that the Kolmogorov backward equation does describe the evolution of a probability distribution backward in time and therefore can also be simulated using particle methods.

3) CONNECTION BETWEEN THE KOLMOGOROV FORWARD EQUATION AND ADVECTION–DIFFUSION EQUATION

As noted before, samples from the probability distribution satisfying the Kolmogorov forward equation can be obtained using a Lagrangian random walk model equation [Eq. (4)]. Here, we establish the connection between the Kolmogorov forward equation [Eq. (1)] and the classical advection–diffusion equation. Our starting point will be the time evolution equation for the concentration of a passive and inert tracer $c(\mathbf{x}, t)$:

$$\frac{\partial c}{\partial t} = -\frac{\partial (u_i c)}{\partial x_i} + \frac{\partial}{\partial x_i}\left(k_{ij}\frac{\partial c}{\partial x_j}\right), \quad c(\mathbf{x}, t=s) = c_0(\mathbf{x}), \quad (7)$$

where $\mathbf{x}$ is the position vector, $\mathbf{u}$ is the fluid velocity, and k_{ij} are the components of the diffusion tensor $\mathbf{K}$. Equation (7) is solved subject to the boundary condition that there is no flux of tracer through the boundary of the domain, that is,

$$\mathbf{n} \cdot (\mathbf{u}c - \mathbf{K} \cdot \nabla c) = 0, \tag{8}$$

with $\mathbf{n}$ being a vector normal to the boundary. For cases where the labeled particles are allowed to leave the domain, the boundary conditions must be modified to either prescribe the flux or the concentration of the label at the boundary. Equation (7) can be rewritten in the form

$$\begin{aligned}\frac{\partial c}{\partial t} &= -\frac{\partial (u_i c)}{\partial x_i} - \frac{\partial}{\partial x_i}\left(c\frac{\partial k_{ij}}{\partial x_j}\right) + \frac{\partial}{\partial x_i}\left(k_{ij}\frac{\partial c}{\partial x_j} + c\frac{\partial k_{ij}}{\partial x_j}\right),\\ &= -\frac{\partial}{\partial x_i}\left[\left(u_i + \frac{\partial k_{ij}}{\partial x_j}\right)c\right] + \frac{\partial^2 (k_{ij} c)}{\partial x_i \partial x_j},\end{aligned} \tag{9}$$

so that we can establish the connection between $\mathbf{a}$ and $\mathbf{b}$ in Eq. (1) and $\mathbf{u}$ and $\mathbf{K}$ in Eq. (7) by identifying

$$\begin{cases} b_{ij} &= k_{ij}, \\ a_i &= u_i + \dfrac{\partial k_{ij}}{\partial x_j}. \end{cases} \tag{10}$$

Substitution of Eq. (10) into Eq. (9) yields the Kolmogorov forward equation [Eq. (1)], and substituting Eq. (10) into Eq. (4) yields the Lagrangian random walk model that is consistent with the advection–diffusion equation [Eq. (7)]. More precisely, we can simulate Lagrangian paths that include the effects of both advection and diffusion using the following Îto stochastic differential equation (SDE):

$$\begin{aligned} d\mathbf{X}(t) = [\mathbf{u}(\mathbf{X},t) + \nabla \cdot \mathbf{K}(\mathbf{X},t)]dt \\ + \boldsymbol{\sigma}(\mathbf{X},t) \cdot d\mathbf{W}(t), \quad \text{for} \quad t \in [s,\infty), \\ \mathbf{X}(t=s) = \mathbf{y}. \end{aligned} \tag{11}$$

Each particle represents a small fraction of the total mass released at the initial time s. By simulating Eq. (11) for many particles, an approximation of the tracer concentration can be obtained (Spivakovskaya et al. 2007a).

The above development shows that the transformation between the probability distribution and the time evolution of a tracer concentration is rather straightforward. The analogy between the randomly moving particles and the spreading of contaminants in a fluid is one of the appealing features of the Lagrangian random walk model. For more details, the reader is referred to Visser (2008), Gräwe et al. (2012), Shah et al. (2011, 2013), and Spivakovskaya et al. (2007a,b).

4) Connection between the Kolmogorov backward equation and the adjoint advection–diffusion equation

There is also a connection between the evolution of $G(t, \mathbf{x}; s, \mathbf{y})$ described by the Kolmogorov backward equation and the evolution of a tracer in the time-reversed adjoint advection–diffusion equation.

To establish the connection, we note that the Kolmogorov backward equation [Eq. (5)] can be rewritten as

$$\frac{\partial G}{\partial s} = -\left(a_i - \frac{\partial b_{ij}}{\partial y_j}\right)\frac{\partial G}{\partial y_i} - \frac{\partial^2}{\partial y_i \partial y_j}(b_{ij} G) + \frac{\partial}{\partial y_i}\left(G\frac{\partial}{\partial y_j} b_{ij}\right). \tag{12}$$

If the flow is divergence free such that

$$\frac{\partial}{\partial y_i}\left(a_i - \frac{\partial b_{ij}}{\partial y_j}\right) = 0, \tag{13}$$

then

$$\frac{\partial}{\partial y_i}\left[\left(a_i - \frac{\partial b_{ij}}{\partial y_j}\right)G\right] = \left(a_i - \frac{\partial b_{ij}}{\partial y_j}\right)\frac{\partial G}{\partial y_i}. \tag{14}$$

Using this equality in Eq. (12) yields

$$\frac{\partial G}{\partial s} = \frac{\partial (\tilde{a}_i G)}{\partial y_i} - \frac{\partial^2}{\partial y_i \partial y_j}(b_{ij} f), \tag{15}$$

where

$$\tilde{a}_i = -a_i + 2\frac{\partial b_{ij}}{\partial y_j}. \tag{16}$$

Now reversing the time by substituting $\tilde{s} = -s$ and defining $\tilde{f}(\tilde{s}, \mathbf{y}; t, \mathbf{x}) \equiv G(t, \mathbf{x}; s = -\tilde{s}, \mathbf{y})$, the above equation takes the form

$$\frac{\partial \tilde{f}}{\partial \tilde{s}} = -\frac{\partial}{\partial y_i}(\tilde{a}_i \tilde{f}) + \frac{\partial^2}{\partial y_i \partial y_j}(b_{ij}\tilde{f}), \tag{17}$$

which is of the same form as the Kolmogorov forward equation [Eq. (1)]. Therefore, it can be solved using a Lagrangian random walk model. In view of Eq. (10), the drift coefficient $\tilde{a}_i$ for the backward problem is given by

$$\tilde{a}_i = -u_i + \frac{\partial b_{ij}}{\partial y_j}, \tag{18}$$

and by letting $v_i = -u_i$, this may be written as

$$v_i = \tilde{a}_i - \frac{\partial b_{ij}}{\partial y_j}. \tag{19}$$

As it turns out, by simply reversing the sign of the velocity field ($v_i \equiv -u_i$) and redefining the time variable ($\tilde{s} \equiv t - s$), we obtain the required Lagrangian random walk model for the backward problem

$$\begin{aligned} d\,\mathbf{Y}(\tilde{s}) = [-\mathbf{u}(\mathbf{Y}, t-\tilde{s}) + \nabla \cdot \mathbf{K}(\mathbf{Y}, t-\tilde{s})]d\tilde{s} \\ + \boldsymbol{\sigma}(\mathbf{Y}, t-\tilde{s})(\mathbf{Y}, t-\tilde{s}) \cdot d\mathbf{W}(\tilde{s}), \quad \text{for} \quad \tilde{s} \in [t, \infty), \\ \mathbf{Y}(\tilde{s}=t) = \mathbf{x}, \end{aligned} \tag{20}$$

where, as before, $d\mathbf{W}$ represents the Wiener increments. Thus, the probability distribution corresponding to the stochastic process $\mathbf{Y}(\tilde{s})$ will be the solution of the adjoint tracer transport equation

$$\frac{\partial \tilde{c}}{\partial \tilde{s}} = -\frac{\partial (u_i \tilde{c})}{\partial y_i} - \frac{\partial}{\partial y_i}\left(k_{ij}\frac{\partial \tilde{c}}{\partial y_j}\right) \tag{21}$$

that was considered in several previous oceanographic applications (e.g., Holzer and Hall 2000; Holzer and Primeau 2006, 2008; Primeau 2005; Primeau and Holzer 2006). We note that Eq. (21) satisfies the incompressibility condition

$$\frac{\partial u_i}{\partial y_i} = 0 \tag{22}$$

that was required to derive Eq. (15) from Eq. (12) as well as the fact that the Kolmogorov equation applied to our problem does indeed describe the backward time evolution of a probability distribution in terms of $\mathbf{y}$. For an application of backward time Lagrangian models in oceanography, the reader is referred to Spivakovskaya et al. (2005).

b. *Probability distributions for the time to transport particles to and from the sea surface*

For the purpose of tracing the movement of water masses to and from the sea surface, it is customary to replace the no flux boundary condition of Eq. (8) with a so-called Dirichlet boundary condition in which the tracer concentration is specified to be zero at the sea surface. At the solid boundaries the no flux boundary condition is retained. In the finite-difference Eulerian tracer transport model, we implement the Dirichlet boundary condition by prescribing the tracer concentration to be zero in the top layer of the model. In the SDE literature (Gardiner 1985), such a boundary condition is known as an absorbing boundary condition. To implement the absorbing boundary condition in the Lagrangian model in such a way that it is consistent with the Eulerian model, we remove particles the first time they cross the boundary separating the bottom of the uppermost layer of the model from the layer immediately below it.

By applying an absorbing boundary condition at the sea surface, the solution to the Kolmogorov equations, which we denote by $G^\circ(t, \mathbf{x}; s, \mathbf{y})$ to distinguish it from the solution with no flux boundary conditions on all boundaries, no longer yields probability distributions for $\mathbf{x}$ and $\mathbf{y}$ because the integral of $G^\circ(t, \mathbf{x}; s, \mathbf{y})$, with respect to $\mathbf{x}$ or $\mathbf{y}$, is no longer normalized to 1. To interpret the solutions to the forward and backward Kolmogorov equations as probability distributions, G° must be normalized appropriately, resulting in

$$P(\mathbf{x} \mid t, s, \mathbf{y}) = \frac{G^\circ(t, \mathbf{x}; s, \mathbf{y})}{\int d\mathbf{x} G^\circ(t, \mathbf{x}; s, \mathbf{y})} \tag{23}$$

for the forward problem and

$$P(\mathbf{y} \mid t, \mathbf{x}, s) = \frac{G^\circ(t, \mathbf{x}; s, \mathbf{y})}{\int d\mathbf{y} G^\circ(t, \mathbf{x}; s, \mathbf{y})} \tag{24}$$

for the backward problem. The probability density function in Eq. (23) gives the probability per unit volume that a particle that was at position $\mathbf{y}$ at time s can be found at position $\mathbf{x}$ at time t without having made contact with the surface during the time interval from s to t. Similarly, the probability density function in Eq. (24) gives the probability per unit volume that a particle that is at position $\mathbf{x}$ at time t could be found at position $\mathbf{y}$ at time s without it having made contact with the surface in the time interval from s to t. As time progresses more and more, particles make contact with the surface and get removed from the flow. The normalization integrals in the denominator of Eqs. (23) and (24), which represent the probability that a particle has not yet been absorbed, gradually decrease to zero. Note that the vertical bar separates the randomly distributed variables (on the left) from the conditioning variables (on the right). This notation, standard for probability theory, expresses a concept that is distinct from the semicolon notation used for the Green functions in the forward and backward Kolmogorov equations. For the Green functions, the semicolon separates the input arguments (on the right) from the output arguments on the left.

An alternative probabilistic interpretation of $G^\circ(t, \mathbf{x}; s, \mathbf{y})$ in terms of last- and first-passage time distributions is also possible (Holzer and Hall 2000;

Primeau 2005). The normalization condition in Eqs. (23) and (24) can be interpreted as the probability that a particle has not yet made contact with the surface, that is,

$$P(t \mid s, \mathbf{y}) = \int d\mathbf{x} G^{\circ}(t, \mathbf{x}; s, \mathbf{y}) \tag{25}$$

is the probability that the particle at position $\mathbf{y}$ at time s will not make contact with the surface in the time interval from s to t, and, similarly,

$$P(s \mid t, \mathbf{x}) = \int d\mathbf{y} G^{\circ}(t, \mathbf{x}; s, \mathbf{y}) \tag{26}$$

is the probability that the particle at position $\mathbf{x}$ at time t did not make contact with the surface in the time interval from s to t. Thus, subtracting these probabilities from unity and differentiating gives the probability density (per unit time) for the last- or first-passage times:

$$P(\tau_{\mathrm{lp}} = t - s; t, \mathbf{x}) = -\frac{\partial}{\partial s}[1 - P(s \mid t, \mathbf{x})] \tag{27}$$

for $s \in (-\infty, t]$, and the first-passage time distribution is given by

$$P(\tau_{\mathrm{fp}} = t - s; s, \mathbf{y}) = \frac{\partial}{\partial t}[1 - P(t \mid s, \mathbf{y})] \tag{28}$$

for $t \in [s, \infty)$. In the above expressions $P(\tau_{\mathrm{lp}}; t, \mathbf{x})$ is the probability density for a particle to have made its last contact with the sea surface at time $s = t - \tau_{\mathrm{lp}}$, conditioned on it being at position $\mathbf{x}$ at time t, and $P(\tau_{\mathrm{fp}}; s, \mathbf{y})$ is the probability density for a particle to make its first contact with the surface at time $t = s + \tau_{\mathrm{lp}}$, conditioned on it having been at position $\mathbf{y}$ at time s. The last-passage time τ_{lp} is usually referred to as the age (e.g., England 1995; Deleersnijder et al. 2001; Delhez and Deleersnijder 2002; Delhez et al. 2004), and $P(\tau_{\mathrm{lp}}; t, \mathbf{x})$ is referred to as the age distribution or as the transit-time distribution (TTD; e.g., Holzer and Hall 2000; Primeau 2005).

In summary, we can compute the first- and last-passage time distributions in two ways:

1) Eulerian method: We solve for $G^{\circ}(t, \mathbf{x}; s, \mathbf{y})$ as a function of $(s, \mathbf{y})$ using the Kolmogorov backward equation with the drift and diffusion given by Eq. (19) and then as a function of $(t, \mathbf{x})$ using the Kolmogorov forward equation with the drift and diffusion given by Eq. (10). With $G^{\circ}(t, \mathbf{x}; s, \mathbf{y})$ in hand, we compute the distributions of last- and first-passage times using Eqs. (27) and (28).
2) Lagrangian method: We initialize an ensemble of Lagrangian particles in the DNP, as shown in Fig. 1 and then use the stochastic differential equations [Eqs. (20) and (11)] to simulate the particles' backward and forward trajectories. We track the particles until they make contact with the surface, at which point we record their surface hitting times. From the sample of hitting times for the backward and forward trajectories, we estimate, respectively, the last- and first-passage time distributions.

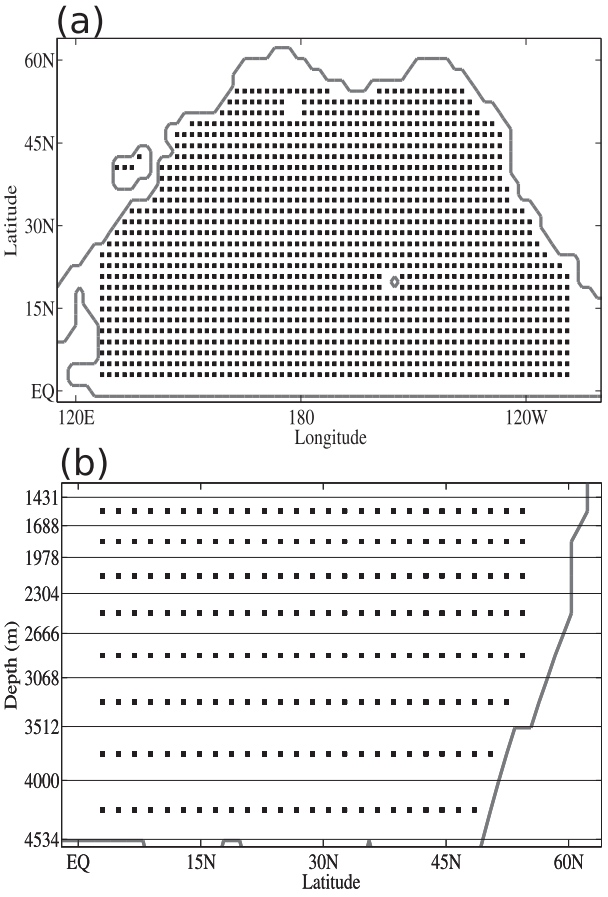

FIG. 1. Initial distribution of tracers in the deep North Pacific. Black squares represent the center of the model's grid boxes; the (a) horizontal section and (b) vertical section of the deep North Pacific Ocean (i.e., below 1431 m). Lagrangian particles are initialized uniformly at the center of each grid box, while the Eulerian tracer is initialized uniformly throughout each grid box. The horizontal solid black lines in (b) shows the edges of the vertical layers. Note that the thickness of the vertical layers varies with depth.

Both methods should give the same result except for the effect of numerical errors.

c. Circulation model

The ocean circulation model with which we compute our tracer diagnostics is based on the formulation described in DeVries and Primeau (2011) and in DeVries (2014). The model has a 2° horizontal resolution with 24 layers in the vertical, ranging in thickness from

approximately 30 m near the surface to 500 m at depth. The dynamical model uses a steady-state linear momentum balance that is optimized to produce a circulation field that reproduces transient CFC-11 observations and climatological observations of salinity, temperature, and natural (prebomb) radiocarbon. The assimilation of these tracers eliminates most of the conspicuous biases that plague free running ocean general circulation models of comparable resolution. More importantly for our application, the assimilation of CFCs and natural radiocarbon ensures that the transport time scales between the DNP and the surface in our circulation model are in agreement with those of the real ocean. Because our dynamical model is used to diagnose the circulation of the ocean by combining observations with the dominant large-scale dynamical balances, we can parameterize the effect of eddies in ways that are not possible or desirable in prognostic OGCMs. An important feature of this model is that the momentum balance includes a forcing term that is used to take into account the various sources of errors in the steady-state linear momentum balance. These include errors due to the missing nonlinear terms, errors in the temperature and salinity observations used to compute the baroclinic pressure terms, errors in the wind forcing, errors due to the missing seasonal cycle, and errors due to missing subgrid-scale physics, including mesoscale eddies. Coarse-resolution prognostic models often include an explicit parameterization for the advective effect of eddies. To the extent that eddy advection leaves an imprint on the tracer fields used for the assimilation, its effect is included in our diagnosed circulation. For our inverse model, separating the velocity field into a large-scale and a subgrid-scale component is an ill-posed problem and is not necessary for the computation of Lagrangian trajectories. For the application of the methods we present here to prognostic ocean circulation models, what is needed is the total advective velocity including both the explicitly resolved large-scale advection and the advection due to subgrid-scale eddies.

The tracer equation parameterizes eddy diffusive fluxes using an isopycnal diffusivity ($K_I = 10^3\,\mathrm{m^2\,s^{-1}}$) with the slope of the isopycnal surfaces computed using climatological observations of temperature and salinity from the *2009 World Ocean Atlas* (Locarnini et al. 2010; Antonov et al. 2010). The vertical diffusivity includes a uniform background vertical diffusivity ($K_V = 10^{-5}\,\mathrm{m^2\,s^{-1}}$) that is enhanced in the surface mixed layer as diagnosed from observations of winter mixed layer depths (de Boyer Montégut et al. 2004) according to the K-profile parameterization of Large et al. (1994).

In comparison to the version of the model used in DeVries and Primeau (2011), substantial improvements have been made to the model. These include (i) a doubling of the horizontal resolution, (ii) a vertical diffusivity that varies in the vertical to account for spatially varying mixed layer depths, (iii) an along-isopycnal diffusivity rather than a horizontal diffusivity, and (iv) the inclusion of CFC-11 in the assimilation.

d. *Numerical setting for the Lagrangian particles and Eulerian tracers*

For the Eulerian diagnostics, we distribute a unit amount of tracer uniformly in a layer bounded by depths between 1431 and 4534 m in the Pacific basin north of the equator, a region we refer to as the deep North Pacific Ocean. The tracer is then propagated backward in time using the adjoint advection–diffusion equation as well as forward in time using the advection–diffusion equation. The time integration scheme used for this computation is a second-order, trapezoidal, Crank–Nicolson method. Both equations are solved subject to a Dirichlet boundary condition in which the surface concentration is prescribed to be zero and no flux boundary conditions at the solid boundaries.

For the Lagrangian diagnostics, we initialize 15 particles at the center of each model grid box within the DNP. Thus, the shallowest particles are initialized at a depth of ~1595 m, and the deepest are initialized at a depth of ~4825 m. Figure 1a shows a plan view of the initial particle locations, and Fig. 1b shows a vertical section view. We simulate a sample of backward and forward Lagrangian trajectories for these particles by applying the Milstein scheme (Shah et al. 2011, 2013) to Eqs. (20) and (11), respectively. As shown in Shah et al. (2011, 2013), it is essential to utilize the Milstein scheme to accurately simulate Lagrangian trajectories in the presence of nonisotropic diffusion. For our ocean circulation model this is particularly important in regions with steep isopycnal surfaces. Furthermore, we used a variable time step size strategy suggested in Shah et al. (2013) to prevent particles from crossing the solid basin boundaries.

Even though we have multiple particles starting at the same location, the stochastic effects that represent the circulation model's eddy diffusivity produces distinctive Lagrangian pathways for each particle. For the deterministic effects of the circulation model's resolved currents, we have to interpolate the velocity available at a set of discrete points centered on the faces of the model's grid boxes onto the locations of the Lagrangian particles. For this, we assume that within a model grid box the x, y, and z components of the velocity vary only in the x, y, and z directions, respectively, and then linearly interpolate each velocity component between grid points. This approach guarantees that the nondivergent

velocity of the ocean circulation model is preserved (Doos 1995). In general, the statistics for an ensemble of trajectories are less sensitive to the interpolation method, provided the integration method is sufficiently accurate. The linear interpolation method has been shown to produce reliable results (Böning and Cox 1988).

3. Results

The waters of the deep North Pacific Ocean are the oldest in the World Ocean (DeVries and Primeau 2011). Given enough time, even relatively weak diapycnal diffusivities become important. We therefore include eddy diffusive effects in the Lagrangian particle trajectories and Eulerian tracer diagnostics we compute. As discussed in section 2, the numerical scheme employed for the computation of the Lagrangian trajectories ensures consistency with the Eulerian tracer diagnostics.

a. Time scales for transport from and to the sea surface

To set a context for the presentation of the Lagrangian ventilation pathways, we begin by reviewing the distribution of times with which particles are transported from the surface to the DNP and back.

The last-passage time distribution is shown in Fig. 2a. The Eulerian and Lagrangian methods for computing the distribution agree reasonably well, considering the numerical errors and the sampling variability associated with the finite sample size used for the Lagrangian method.

To first order we see that the most probable last-passage time from the surface for water particles in the DNP (i.e., the most probable age) is ~600 yr, but the distribution is strongly skewed to the right. The mean of the distribution is ~1172 yr. An eigenanalysis of the adjoint transport operator reveals that the tail decays exponentially with a time scale of 783 yr as $\tau_{lp} \to \infty$. The exponentially decaying tail of the last-passage distribution is in clear opposition to the "great ocean conveyor" metaphor (Broecker 1991), which at face value predicts a sharp cutoff for the maximum age of water parcels. The exponential decay of the age distribution for large age values has been noted previously in Mouchet et al. (2012) and Primeau and Holzer (2006). The exponential tail of the age distribution is a manifestation of eddy mixing, which, by imparting a random walk component to particle trajectories, gradually erases a particle's memory of its past trajectory. As pointed out by Primeau and Holzer (2006), for particles that reside in the ocean a very long time, this loss of memory causes the ocean to look progressively more like a well-mixed reservoir, for which the age distribution is an exponentially decaying function (Bolin and Rodhe 1973). In section 3c, we illustrate with explicit examples of particle trajectories with long surface-to-DNP transit times how large-scale advection coupled to eddy-driven random walk behavior produces this loss of memory.

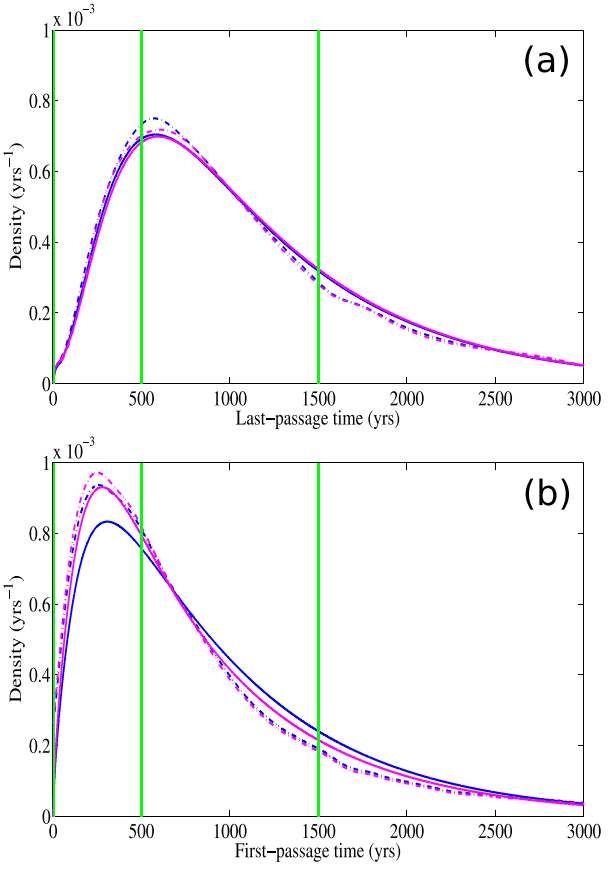

FIG. 2. (a) Distribution of last-passage times (also known as the age distribution or the transit-time distribution) and (b) distribution of first-passage times for the deep North Pacific Ocean region as computed using the Eulerian tracer method (solid) and using the Lagrangian particle model (dashed). Distributions in blue are computed for DNP, while distributions in magenta are recomputed for the tracer initialized above ~4000 m in DNP (i.e., by excluding the deepest DNP layer). The vertical green lines separate the time intervals used in the ventilation diagnostics of sections 3b and 3c.

The first-passage time distribution is shown in Fig. 2b. Unlike the case of the last-passage time distribution, here we see a substantial discrepancy between the Lagrangian and Eulerian results. The most probable arrival time as estimated from the Lagrangian calculation is ~250 yr, whereas the Eulerian calculation suggests that the most probable arrival time is closer to ~300 yr. But more importantly, the Lagrangian calculation suggests

that a larger fraction of the particles are transported along fast trajectories than implied by the Eulerian calculation. This difference is too large to be attributed to the distinct and unavoidable discretization errors tied to each method. Further investigation reveals that the difference can be attributed to the fact that the initial positions of the Lagrangian particles are not distributed uniformly in the DNP. Because the particles are initialized in the middle of the model layers and the thickness of model layers increase with depth, the number of particles initialized per unit volume decreases with depth. This, together with the fact that the mean first-passage time in the North Pacific increases monotonically with depth (DeVries and Primeau 2011), explains the bias toward shorter first-passage times in the Lagrangian calculation. For the last passage we did not obtain a biased result because the depth of the maximum mean age is located at a depth with approximately the same number of particles initialized above and below the maximum. In support of this explanation, we recomputed the first-passage time distribution using only particles initialized above 4000 m instead of 4534 m, that is, by excluding the deepest and thickest DNP layer (Fig. 1b) found that the bias was greatly reduced (Fig. 2). To avoid such biases, future applications of the Lagrangian method should initialize particles uniformly within the starting domain of interest, perhaps by randomly distributing the particles inside the starting volume.

Ignoring the remaining minor differences between the Lagrangian and Eulerian calculations, we see that the first-passage time distribution is skewed to the right with a mean of ~951 yr and a mode at only 300 yr. For $\tau_{\mathrm{fp}} \to \infty$, the first-passage time distribution enters an exponentially decaying regime with an *e*-folding decay time scale of 783 yr. This *e*-folding time scale is identical to that of the last-passage time distribution. However, the exponentially decaying regime of the first-passage time distribution accounts for ~11% fewer particles than it does for the last-passage time distribution. As we will see in the next section, this difference together with the shift of the mode and mean to shorter times relative to the last-passage time distribution can be explained by the fact that particles can be flushed out of the DNP along relatively short pathways to the nearby upwelling regions of the equatorial Pacific Ocean.

b. *Locations where particles make their last and first contact with the surface ocean*

To explore the relative importance of different surface regions for the ventilation of the deep North Pacific Ocean, we recorded the surface hitting locations of the backward and forward particle trajectories. The surface hitting locations for the backward trajectories correspond to regions that contribute to the formation of the water masses residing in the DNP, whereas the surface hitting locations for the forward trajectories correspond to regions where water from the DNP is first exposed to the atmosphere. These surface hitting locations are shown in Fig. 3.

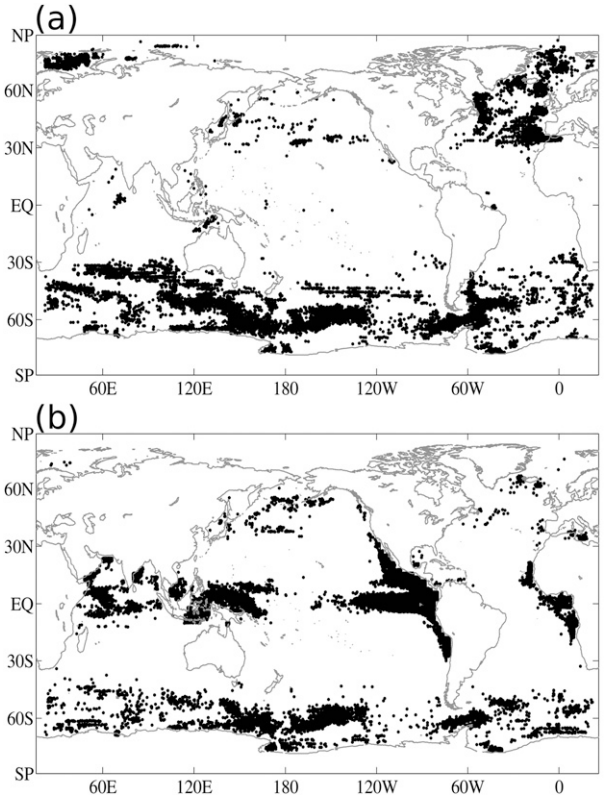

FIG. 3. Surface hitting locations for deep North Pacific particles (a) showing where particles last hit the surface before being transported to the DNP (i.e., surface locations where tracers enter the deep Pacific ocean) and (b) showing where particles in the DNP will first hit the surface (i.e., locations where deep Pacific tracers are first exposed to the atmosphere). Of initial populations of 146 340 particles, only particles with last- or first-passage times less than 3000 yr are shown.

The main regions where DNP waters enter the interior as they begin their journey to the North Pacific are in the Southern Ocean and in the North Atlantic Ocean. The contribution from the surface of the North Pacific Ocean is relatively minor despite its proximity to the DNP. This is in accord with the fact that there is no deep water formed in the North Pacific Ocean.

For the reexposure of DNP waters to the atmosphere, the main regions are in the tropical Indian, Pacific, and eastern Atlantic basins as well as in the Southern Ocean. Because of wind-driven Ekman upwelling along the coast of the Americas, the region with a high density of first contacts in the eastern tropical Pacific extends to the

north and south into the subtropics. A significant number of the particles from our sample also make their first contact with the surface in the western part of the Pacific Subpolar Gyre where Ekman divergence and deep mixed layers brings particles to the surface. In contrast, none of the particles in our sample hit the surface in the subtropical gyres where Ekman convergence drives downwelling currents.

In comparing the maps of the backward and forward hitting locations, the Southern Ocean stands out as a region that is important for both connecting pathways from the surface to the DNP and from the DNP back to the surface. However, the forward hitting locations are confined farther south in the region of Antarctic divergence, whereas the backward hitting locations extend farther north into the Antarctic and subtropical convergence zones.

Using the Eulerian model, we computed the spatial probability distribution for the backward and forward hitting location partitioned according to fast (τ_{lp}, $\tau_{fp} <$ 500 yr), intermediate (500 $< \tau_{lp}$, $\tau_{fp} <$ 1500 yr), and slow (τ_{lp}, $\tau_{fp} >$ 1500 yr) pathways. The breakdown into fast, intermediate, and slow pathways for the backward trajectories accounts for approximately 21%, 54%, and 25% of the water mass, and for the forward trajectories it accounts for approximately 34%, 47%, and 20% of the water mass. The results for the backward trajectories are shown in the left panels of Fig. 4, and the results for the forward trajectories are shown in the right panels.

The probability density of last contact with the surface is relatively more localized than the corresponding probability for first contact. This is most evident by comparing the latitudinal probability densities for the last and first contact with the surface shown in Fig. 4. The high probability density centered at the equator dominates the first-contact probability density but is absent in the distribution for the location of last contact with the surface.

Only approximately 4% of the DNP water is ventilated from the surface North Pacific with most of this coming from fast and intermediate pathways. Approximately 67% of the DNP water is ventilated from the Southern Ocean, with a 15.6%, 35.4%, and 16.3% breakdown into fast, intermediate, and slow pathways. The remaining water, approximately 27% of the DNP volume, is ventilated from the high-latitude North Atlantic with a 2.9%, 15.5%, and 8.2% breakdown into fast, intermediate, and slow pathways. Not surprisingly, considering the greater distance separating the North Atlantic from the North Pacific, the breakdown for the North Atlantic skews toward more intermediate and slow pathways compared to the Southern Ocean.

Approximately 42% of the DNP water is first reexposed to the atmosphere in the low-latitude ocean between 30°S and 30°N, and most of these pathways (~80%) make their first contact in the Pacific sector. For the low-latitude region there is a 15.9%, 18.7%, and 7.5% breakdown into fast, intermediate, and slow pathways. Approximately 30% of the DNP water is first reexposed in the Southern Ocean, with a 7.4%, 15.7%, and 7.3% breakdown into fast, intermediate, and slow pathways. Most of the remaining DNP water (27%) makes its first contact with the surface north of 30°N in the Pacific Ocean, with a 10.2%, 12.7%, and 4.7% breakdown into fast, intermediate, and slow pathways. As expected, because of the shorter distances, we find a relatively larger proportion of fast and intermediate pathways for the north and low-latitude Pacific Ocean compared to the Southern Ocean. The relatively larger role played by the Southern Ocean for the slow paths is also evident in the zonal probability profiles for the first contact in Fig. 4. For first-passage times greater than 1500 yr, the Southern Ocean mode has the highest density, whereas for first-passage times less than 500 yr, it is the smallest of the three peaks.

c. *Ventilation pathways of the deep North Pacific Ocean*

In this section, we present a sample of Lagrangian pathways of water particles as they are transported by eddies and the mean circulation from the surface to the deep North Pacific and from the deep North Pacific back to the surface. We partition these pathways according to their surface hitting location as well as into groups of fast, intermediate, and slow pathways as we did in section 3b.

1) SURFACE TO DEEP NORTH PACIFIC PATHWAYS

(i) North Atlantic surface to DNP pathways

Three sample pathways connecting the surface of the North Atlantic to the DNP are shown in Fig. 5. The first particle, whose path is shown in Fig. 5a, follows a pathway very similar to that suggested by the abyssal circulation sketched in Stommel (1958). It starts to the west of Iceland and drifts westward into the Labrador Sea where it convects down to a depth of ~1400 m. It then does a loop in the subpolar gyre of the North Atlantic where it is upwelled back to depths of ~200 m before being subducted down to depths of more than ~800 m. The particle then drifts southward, first in the center of the North Atlantic and then westward where it is entrained into the deep western boundary current. It is then transported quickly southward where it joins the Antarctic Circumpolar Current (ACC). The particle is then quickly detrained into the Pacific basin where it follows a northward pathway into the DNP. The total

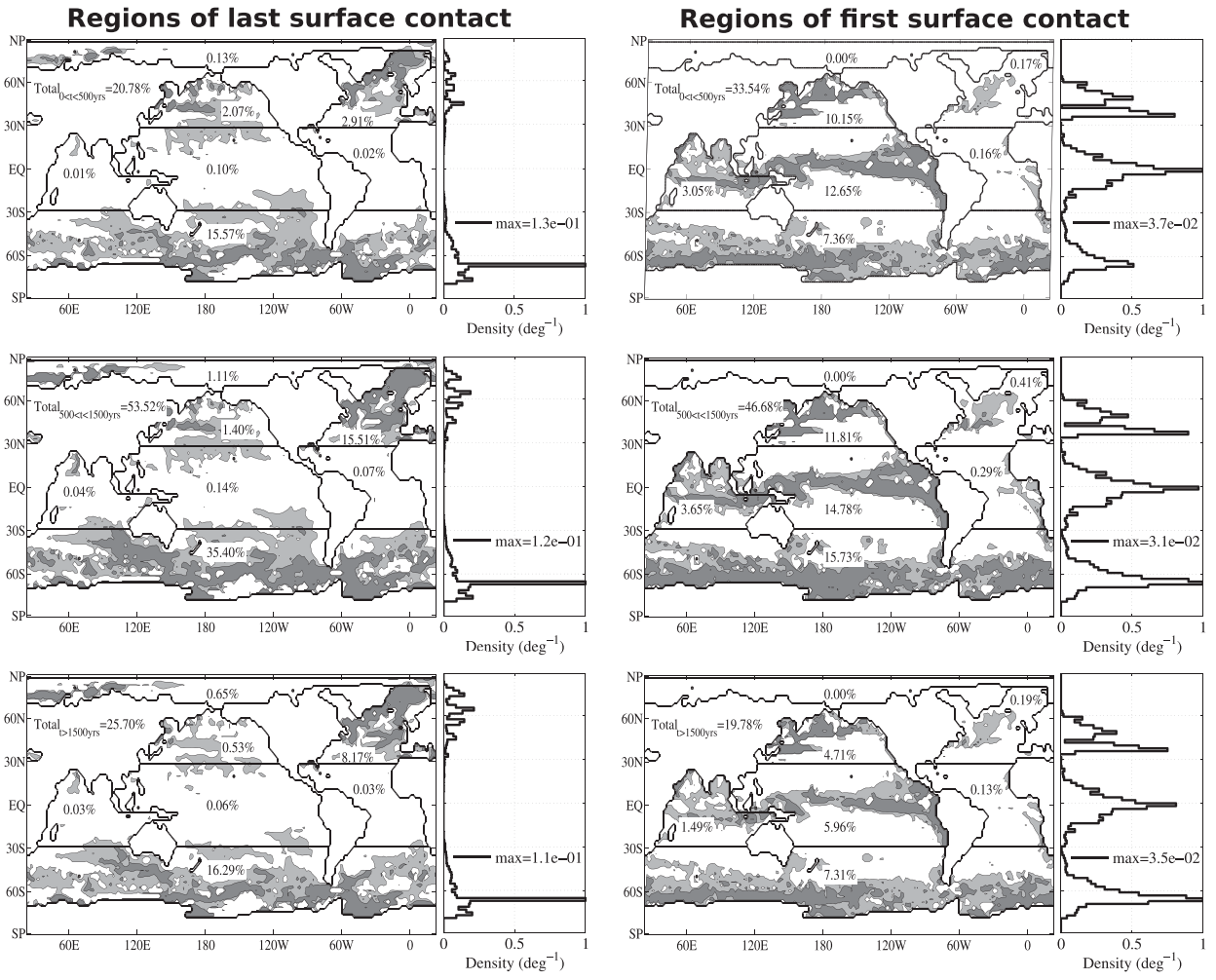

FIG. 4. Fraction (%) of deep North Pacific water that made its (left) last contact and (right) first contact with the surface partitioned into seven regions separated by the black lines. The filled contours represent probability contours 10^{-15} and 10^{-16}. The profiles to the right of the maps show the probability density (normalized by their maximums) for the latitude of last contact with the surface. The uppermost panels correspond to fast paths with $0 < \tau_{lp}, \tau_{fp} < 500$ yr. The middle panels correspond to intermediate paths with $500 < \tau_{lp}, \tau_{fp} < 1500$ yr. The bottom panels correspond to slow paths with $\tau_{lp}, \tau_{fp} > 1500$ yr. Displayed over Asia is the fraction (%) of the DNP water accounted for by each time interval.

transit time for the particle is 295 yr, of which 241 yr are spent at depths below 1500 m.

The second particle, whose path is shown in Fig. 5b, starts in the western North Atlantic and does several loops around the subtropical gyre at depths above 500 m before being transported into the subpolar gyre where it does several more loops at depths greater than 500 m. Eventually the particle is transported southward in the eastern part of the Atlantic basin before drifting westward and joining the deep western boundary current near 20°N. The particle then flows southward and along the equator before crossing into the South Atlantic in the eastern part of the basin. By this time the particle is already 250 years old. The particle then follows a southward path where it joins the ACC. After three full circuits around the ACC the particle is detrained into the Pacific where it then follows an eddying path into the eastern North Pacific. The total transit time is 959 yr, of which 591 yr were spent at depths greater than 1500 m.

The third particle, illustrating the pathways connecting the surface North Atlantic to the DNP (Fig. 5c), starts to the southwest of Iceland where it circulates in the North Atlantic at relatively shallow depths before convecting to depths greater than 1000 m in the Labrador Sea. The particle then follows a southward pathway down the eastern Atlantic basin before being entrained into the ACC where it is quickly detrained into the Pacific basin. It then follows a northward pathway into the

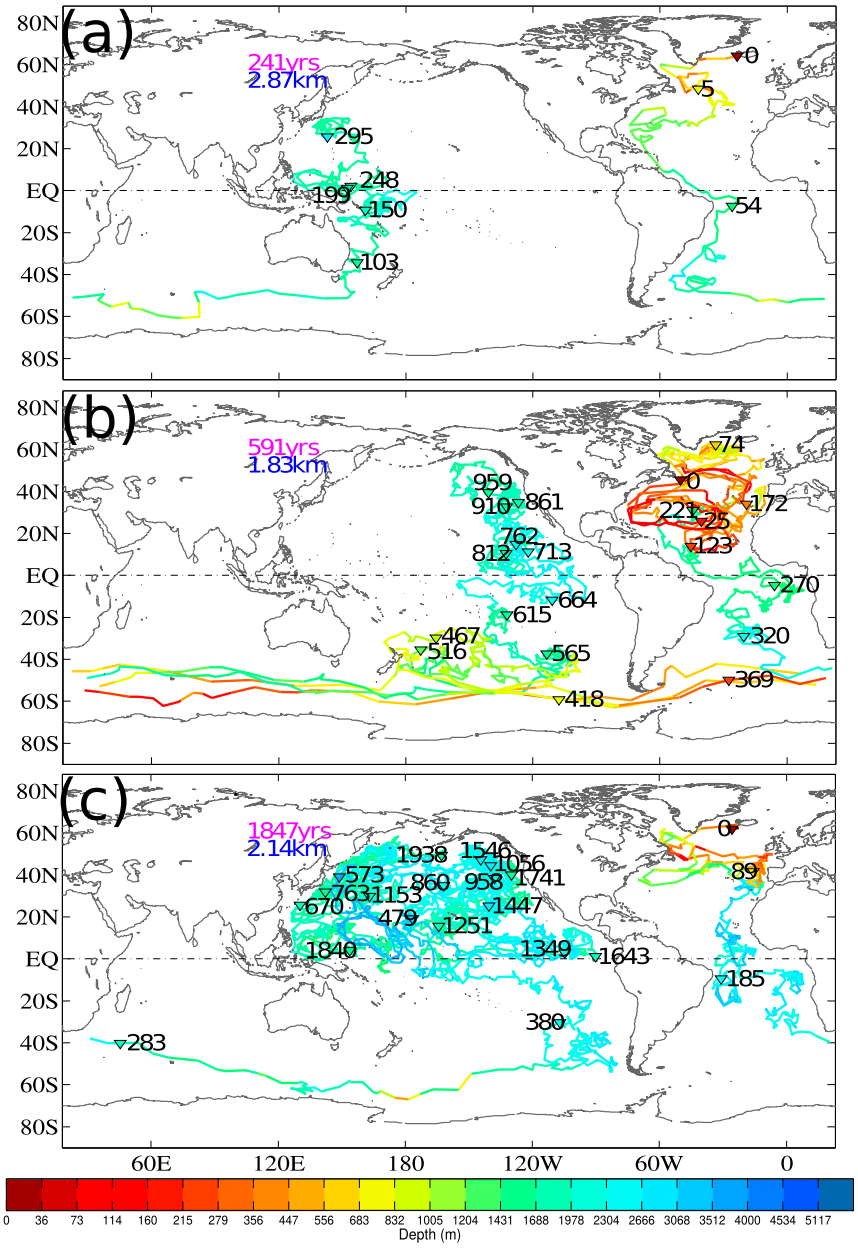

FIG. 5. A sample of Lagrangian pathways whose last contact with the surface was in the North Atlantic for (a) a fast ($\tau_{lp} < 500$ yr), (b) an intermediate ($500 < \tau_{lp} < 1500$ yr), and (c) a slow 1500 yr $< \tau_{lp}$ particle. These trajectories are computed backward in time using a backward Lagrangian model with the particle initialized in the DNP at terminal time. The blue number indicated over Asia represents the initial depth of the particle. The instantaneous age of the particle is given by subtracting the time indicated by the numbers (yr) beside the ∇ from the largest such time, that is, from the time at which the particle hits the surface. The color represents the depth of the particle. The magenta number indicated over Asia represents the total time spent by the particle below 1500 m.

DNP. By the time the particle has reached an age of ~450 yr it is already in the North Pacific where it follows a random walk north of the equator for the remaining 1500 yr. This particle trajectory illustrates how much of the aging of the waters in the DNP occurs in the deep North Pacific basin itself. The total transit time for this particle is 1938 yr, of which 1847 are spent at depth greater than 1500 m.

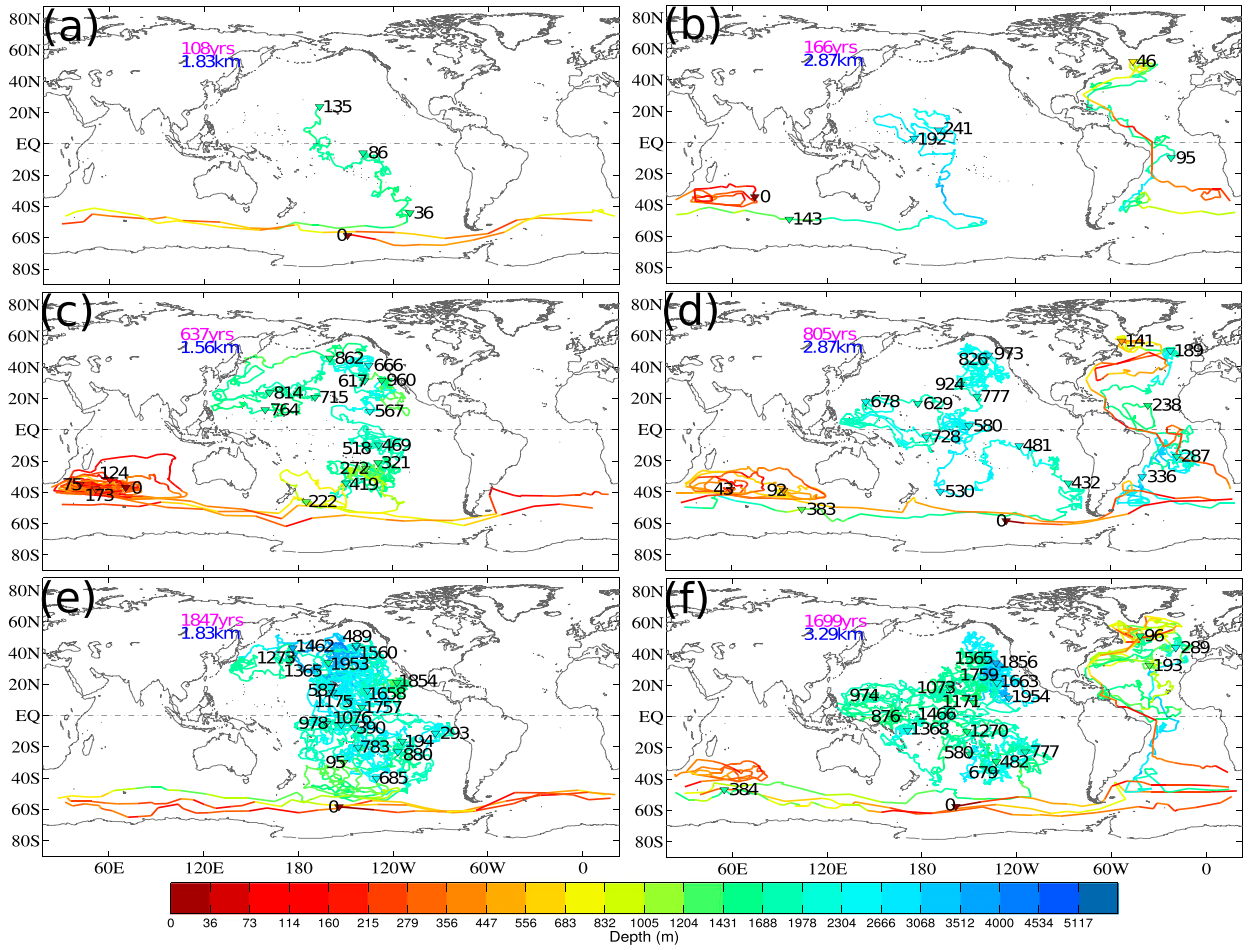

FIG. 6. As in Fig. 5, but for Lagrangian pathways whose last contact with the surface was in the Southern Ocean. Panels (a) and (b) correspond to fast pathways. Panels (c) and (d) correspond to intermediate pathways and panels (e) and (f) correspond to slow pathways.

(ii) Southern Ocean surface to DNP

Six sample pathways for particles that are transported from the surface of the Southern Ocean to the DNP are shown in Fig. 6. Figures 6a and 6b show fast particles, one of which does two circuits around the ACC at shallow to intermediate depths before being detrained into the Pacific after ~36 yr. It then follows a pathway to the North Pacific for a total transit time of 135 yr, of which 108 yr were spent below 1500 m. The second particle in our sample starts in the Indian Ocean sector of the Southern Ocean where it does several loops in the subtropical gyre of the Indian Ocean before contributing to the Agulhas leakage into the Atlantic basin where it flows northward in the upper ocean into the high-latitude North Atlantic. It then returns southward along the deep western boundary current, is entrained into the ACC, and quickly detrained into the Pacific basin where if flows northward into the DNP. The total transit time is 241 yr, of which 166 yr were spent below 1500 m.

Figures 6c and 6d show two intermediate pathways that start in the Southern Ocean. Both pathways in our sample do several loops around the subtropical gyre of the Indian Ocean as well as two full circuits around the ACC. The particle pathway in Fig. 6c does not contribute to the Agulhas leakage; instead, it gets entrained into the ACC where it does two full circuits before drifting into the South Pacific where it spends ~250 yr before crossing the equator and doing a random walk in the DNP for another ~400 yr. In total, the particle takes 960 yr to be transported from the surface of the Indian Ocean sector of the Southern Ocean to the DNP. Of those 960 yr, 637 yr are spent at depths below 1500 m. The particle pathway in Fig. 6d that does contribute to the Agulhas leakage flows northwestward across the South Atlantic before crossing the equator in the

western boundary. It then flows northward, does a loop around the subtropical gyre of the North Atlantic, and drifts into the Labrador Sea where it is convected to depth. By this time the particle is ~100 years old. The particle then does a random walk southward in the deep Atlantic basin, rejoins the deep ACC, and drifts into the Pacific off the coast of Chile. The particle then does a random walk for another ~550 yr up into the Gulf of Alaska. The total transit time for this particle is 973 yr, of which 805 yr are spent below 1500 m.

Finally, Figs. 6e and 6f show slow pathways. The particle pathway shown in Fig. 6e drifts into the Pacific basin after executing three circuits around the ACC at shallow to intermediate depths before drifting into the Pacific basin where it performs a random walk for more than ~1850 yr. The particle pathway shown in Fig. 6f makes an excursion into the Atlantic basin by way of the Agulhas leakage. In the Atlantic the particle flows northward in the upper ocean all the way to the deep convection regions of the North Atlantic before returning southward at depth where the particle is reentrained into the ACC and then detrained into the Pacific where it executes a random walk into the DNP. The total transit time from the surface of the Southern Ocean to the DNP is 1954 yr, of which 1699 are spent at depth greater than 1500 m.

2) Deep North Pacific to surface ocean

For every particle that makes its way from the surface to the DNP a particle in the DNP must be flushed out and transported back to the surface. Of course the time scales and pathways for the transport back to the surface are quite different. The surface hitting locations for the return pathways are much less localized then the formation region, which were largely limited to the North Atlantic and Southern Ocean. In Figs. 7, 8, and 9, we show a sample of fast, intermediate, and slow particle pathways from the DNP to the surface. These figures are organized in terms of the basin where the particles make their first contact with the surface. Figure 7 shows a sample of pathways for particles that make first contact in the Indian (Figs. 7a–c) and Southern Oceans (Figs. 7d–f). Figure 8 shows a sample of pathways that make their first contact in the eastern South Pacific in the upwelling region off the coast of South America (Figs. 8a–c) and in the eastern South Atlantic basin in upwelling region off the coast of Africa (Figs. 8d–f). Finally, Fig. 9 shows a sample of pathways that make first surface contact in the North Atlantic (Figs. 9a–c) and North Pacific (Figs. 9d–f) basins.

(i) DNP to Indian Ocean surface

Of the particles that make first contact in the Indian Ocean Basin in our sample (Figs. 7a–c), the fast and intermediate pathways reach the Indian Ocean through the Indonesian Throughflow. Both particles recirculate south of equator by following the South Equatorial Current and the Equatorial Countercurrent before drifting into the Arabian Sea where it upwells to the surface. The total transit time for the fast pathway is 247 yr, of which 65 yr are spent at depths greater than 1500 m. The total transit time for the intermediate pathway is 904 yr, of which 749 yr are spent at depths greater than 1500 m. The slow pathway follows a random walk that eventually allows it to be entrained into the ACC where it travels twice around Earth. To the south of Tasmania the particle is entrained into the northeastward branch of the Indian Subtropical Gyre, which carries it across the Indian Ocean basin to the coast of Africa before turning eastward along the equator and eventually following a random walk into the Bay of Bengal where it is upwelled to the surface. The total transit time for the slow pathway is 2036 yr, of which 1860 yr are spent below 1500 m.

The three particles in our sample that make first contact with the surface in the Southern Ocean (Figs. 7d–f) follow random walks from the DNP to the Southern Ocean where the particles are entrained into the ACC. The fast pathway does one full circuit around the ACC before hitting the surface after a total DNP-to-surface transit time of 143 yr, of which 115 yr were spent below 1500 m. The intermediate pathway also does one circuit around the ACC, except that before upwelling to the surface it executes a random walk in the deep Southern Ocean between Africa and Australia, which adds ~100 yr to the transit time. The total transit time of the intermediate pathway is 560 yr, of which 492 yr are spent below 1500 m. The slow pathway reaches the ACC after a random walk in the Pacific basin that lasts about 1950 yr. Once in the ACC, the particles do two full circuits around Earth before hitting the surface. The total transit time for the slow pathway is 2044 yr, of which 1896 yr are spent at depths greater than 1500 m.

(ii) DNP to eastern boundary upwelling regions of the South Pacific Ocean

We show three pathways that connect the DNP to surface first-contact locations along the eastern boundary upwelling regions of the South Pacific Ocean. The fast pathway (Fig. 8a) follows a random walk from the central subpolar gyre to the western boundary where it recirculates at depths for ~100 yr before being carried southward to the equator where it is entrained into the Equatorial Undercurrent, which carries it quickly across the basin. The particle is then carried southward before upwelling along the coast of Chile. The total

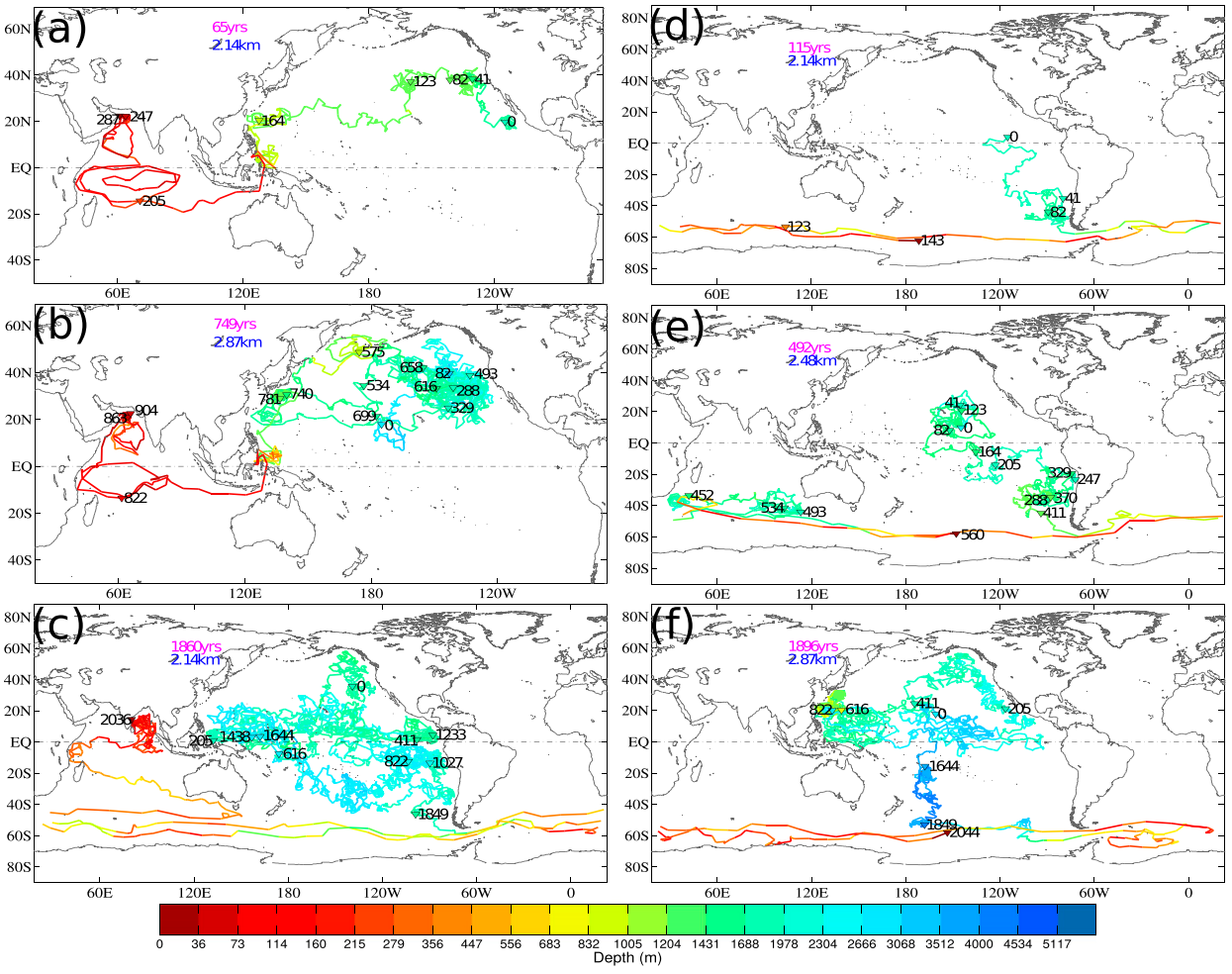

FIG. 7. As in Fig. 6, but for particles that make their first contact with the surface of the (left) Indian and (right) Southern Oceans.

DNP-to-surface transit time for this particle is 215 yr, of which 166 yr are spent at depths greater than 1500 m.

The intermediate pathway (Fig. 8b) executes random walk in the DNP before crossing into the Indian Ocean Basin via the Indonesian Throughflow. The particle then recirculates in the Indian Ocean around the South Equatorial Current and the South Equatorial Countercurrent at shallow depths as well as around the South Indian Subtropical Gyre at intermediate depths. The particle is then entrained into the ACC and is quickly detrained into the western South Pacific where it makes the first contact with the surface off the coast of Chile. The total transit time is 575 yr, of which 298 yr are spent at depths greater than 1500 m.

Finally, the slow pathway (Fig. 8c) follows a southward pathway into the Southern Ocean, where it drifts westward. From there it makes a brief excursion into the South Atlantic followed by a random walk excursion into the western Indian Ocean that lasts more than 1000 yr. The pathway then rejoins the ACC before reentering the Pacific Ocean east of Australia. The pathway follows a pathway north up to the equator where it veers eastward and crosses the equator in the eastern Pacific Ocean. The particle then returns close to its starting position but approximately 1200 m higher up in the water column. The particle then drifts westward and upwells into the Equatorial Undercurrent close to the Maritime Continent and is carried across the Pacific basin and down the coast of South America before hitting the surface off the coast of Chile. The total transit time for this particle is 1728 yr, of which 1455 yr are spent at depths greater than 1500 m.

(iii) DNP to eastern boundary upwelling region of the Atlantic Ocean

For the particles that hit the surface in the Atlantic eastern boundary upwelling region, the fast pathway (Fig. 8d) follows a pathway southward from the DNP to

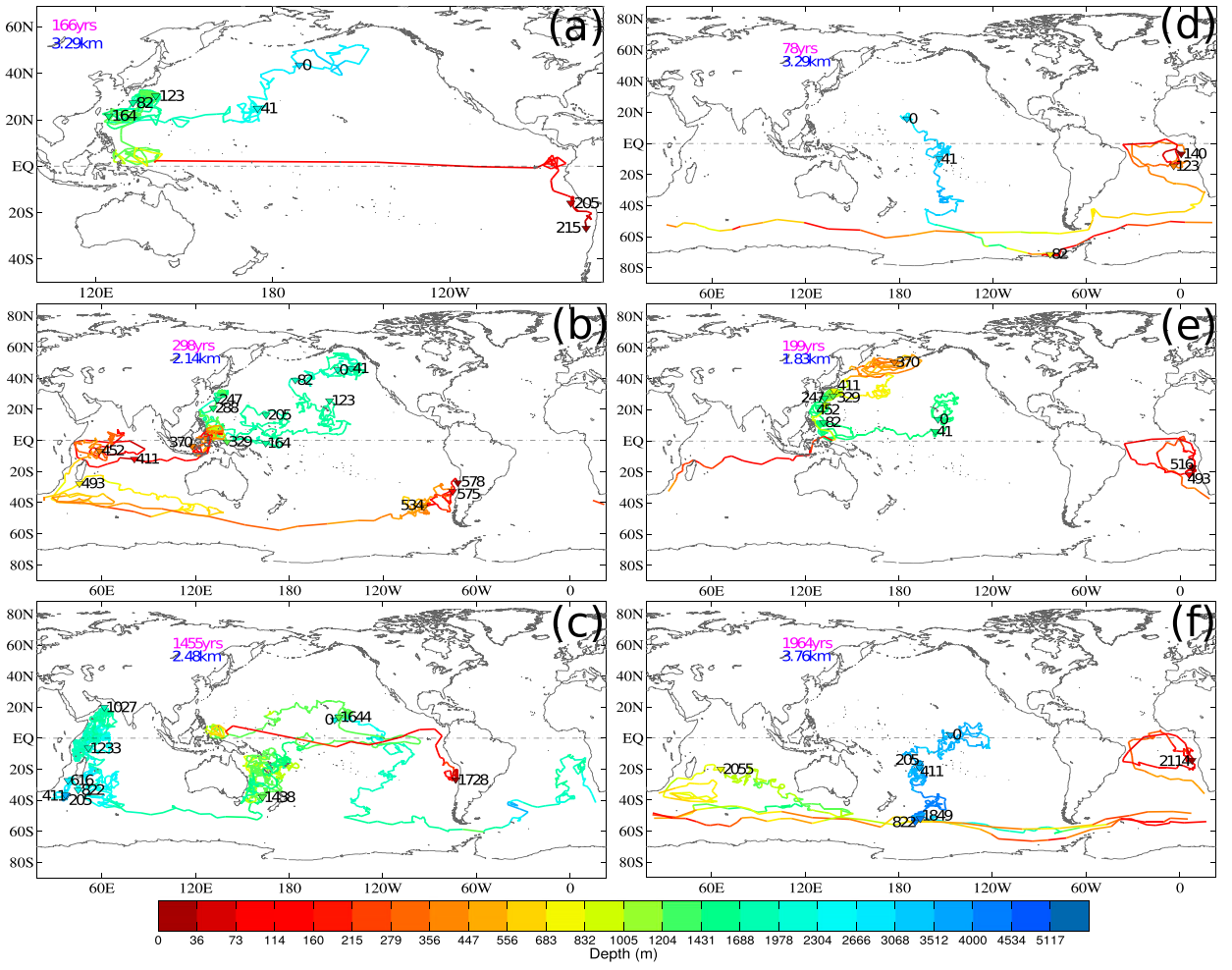

FIG. 8. As in Fig. 6, but for particles that make their first contact with the surface in the eastern boundary upwelling regions of the (left) Pacific and (right) South Atlantic basins.

the Southern Ocean at depth where it is mixed into the upper ocean along the coast of Antarctica. The particle then journeys around the ACC before being entrained into the South Atlantic near the tip of South Africa. From there the particle drifts northwestward in the South Atlantic Subtropical Gyre at a depth of ~500 m. Near the western boundary the particle turns northward and spirals up to the surface following the Equatorial Undercurrent eastward and the South Equatorial Current westward before hitting the surface near the coast of Angola.

The intermediate pathway (Fig. 8e) follows a path in the North Pacific for approximately 500 yr before escaping into the Indian Ocean via the Indonesian Throughflow. The particle then rapidly crosses the Indian Ocean Basin at relatively shallow depths before rounding the tip of Africa into the Atlantic basin. From there, the particle follows a pathway very similar to the fast particle. The total transit time from the DNP to the surface hitting location near the coast of Angola for the intermediate pathway is 516 yr, of which 199 yr were spent at depths greater than 1500 m.

The slow pathway (Fig. 8f) follows a random walk from the DNP to the Southern Ocean in the abyssal ocean. In the Southern Ocean, the particle executes three full circuits around Earth before drifting into the Indian Ocean where the particles follow a pathway into the subtropical gyre of the Indian Ocean at depths of ~1100 m. The particle then recirculates into the subtropical gyre before leaking into the Atlantic basin where it follows a pathway very similar to the intermediate and fast particles described above. The total DNP-to-surface transit time for the slow pathway is 2114 yr, of which 1964 yr are spent at depths greater than 1500 m.

(iv) DNP to North Atlantic surface

The particles that make first contact with the North Atlantic region (Figs. 9a–c) all travel around the ACC

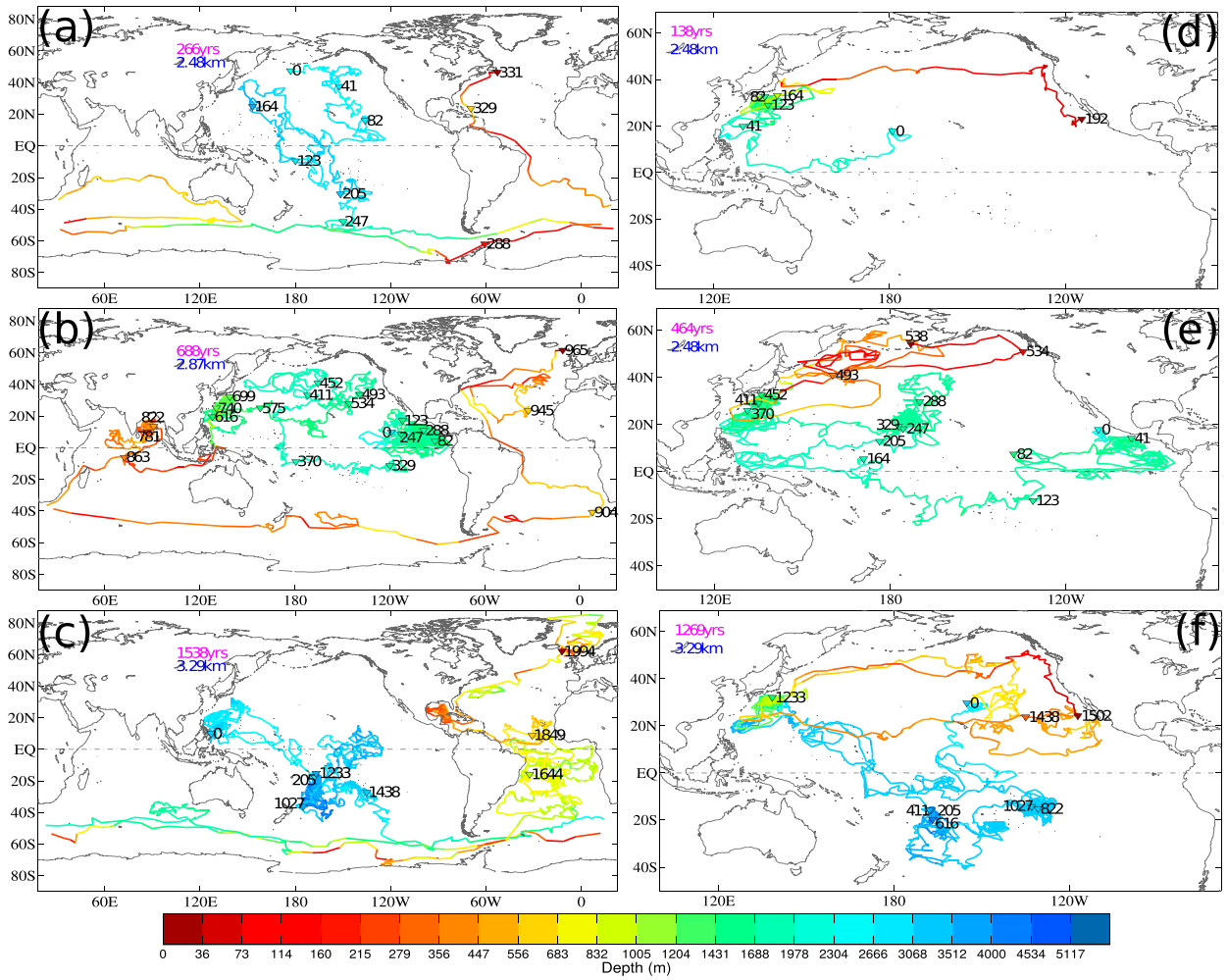

FIG. 9. As in Fig. 6, but for particles that make their first contact with the surface in the eastern boundary upwelling regions of the (left) North Atlantic and (right) North Pacific basins.

before drifting into the high-latitude North Atlantic via the western boundary current in the upper ocean. The fast and slow particle both follow a random walk from the DNP to the Southern Ocean in the deep Pacific Ocean, while the intermediate pathway leaves the Pacific via the Indonesian Throughflow at relatively shallow depths.

Apart from its two circuits around the ACC, the fast particle (Fig. 9a) does an excursion in the Indian Ocean Subtropical Gyre before escaping into the Atlantic via the Agulhas leakage. The total transit time for the fast particle is 331 yr, of which 266 yr are spent at depths greater than 1500 m.

After crossing into the Indian Ocean, the intermediate pathway (Fig. 9b) makes an excursion into the Bay of Bengal before crossing the Indian Ocean and drifting south via the Agulhas Current. At the southern tip of Africa, the pathway retroflects and drifts westward in the upper water column of the ACC before being entrained into the subtropical gyre of the South Atlantic Ocean. The particle then follows the western boundary current northward across the equator, does one circuit around the subtropical gyre of the North Atlantic, and makes its first contact east of Iceland. The total transit time for the intermediate pathway is 965 yr, of which 688 yr are spent at depths greater than 1500 m.

The slow pathway (Fig. 9c) performs a random walk of more than 1200 yr in the abyssal waters of the South Pacific before being entrained into the ACC. The particle is then detrained into the South Atlantic Ocean where it performs another random walk of a few hundred years at depths near 1000 m. The particle then crosses the equator and flows northward along the western boundary current and the North Atlantic current where it makes contact with the surface to the east

of Iceland after a total transit time of 1994 yr, of which 1538 yr were spent at depths greater than 1500 m.

(v) DNP to North Pacific surface

In our illustrative sample of DNP-to-surface pathways, we have a fast and a slow trajectory (Figs. 9d,f) hitting the surface in the eastern boundary upwelling regions off the shore of Baja California, and one intermediate pathway (Fig. 9e) hitting the surface in the Gulf of Alaska.

The fast pathway (Fig. 9d) begins in the tropical central Pacific Ocean and drifts southwestward until it reaches the western boundary where it turns northward, executing an eddying random walk at nominal depths of ~2500 m before being upwelled to the upper ocean near the boundary separating the subtropical and subpolar gyres of the North Pacific. The pathway then crosses the Pacific Ocean carried by the Kuroshio Extension system before turning southward along the coast of North America. The total transit time is 192 yr, of which 138 yr are spent below 1500 m.

The intermediate pathway (Fig. 9e) begins near the eastern boundary of the North Pacific and follows a random walk in the deep ocean (depths > 1500 m) before being upwelled into the upper ocean near the coast of Japan. The pathway then does several loops around the subpolar gyre and one loop around the subtropical gyre before hitting the surface. The total transit time is 538 yr, of which 464 are spent at depths greater than 1500 m.

Finally, the slow pathway (Fig. 9f) executes a random walk in the deep ocean that crosses the equator multiple times before being upwelled to the upper ocean in the western Pacific basin where the Kuroshio separates from the coast. The pathway then does a large loop around the subtropical gyre that includes a lengthy random walk at depths near ~750 m. The pathway eventually hits the surface after traveling southward along the eastern boundary upwelling region. The total transit time for the slow pathway is 1502 yr, of which 1269 yr are spent below 1500 m.

4. Summary and conclusions

Using a combination of Lagrangian and Eulerian tracers we have quantified the ventilation pathways and time scales of the deep North Pacific Ocean (DNP). Because the oldest waters of the World Ocean are located in the DNP, the pathways we have computed trace many of the circulation branches illustrated in schematic diagrams of the great ocean conveyor (Richardson 2008). Unlike the schematic diagrams, which, by emphasizing the mean transport, show smooth arrows that give the impression of laminar flow, the stochastic components introduced in our Lagrangian particles remind us that the ocean is a turbulent fluid. As emphasized in the introduction, previous Lagrangian calculations (Fujio and Imasato 1991; Fujio et al. 1992; Böning and Cox 1988; Doos 1995) have neglected the effect of eddy diffusion on the movement of particles, but diffusive effects cannot be ignored. Indeed, Talley (2013) has emphasized the importance of diffusion for the closure of the global overturning circulation.

The background vertical diffusivity used in our inverse circulation model ($10^{-5}\,m^2\,s^{-1}$) is consistent with the best estimates of the global-averaged diapycnal diffusivity for above depths of 1000 m but is an order of magnitude lower than the best global-averaged estimates below 1000 m (Waterhouse et al. 2014). By taking into account the three-dimensional nature of the global circulation, the inverse model was able to find a climatological circulation state that is consistent with independent estimates of air–sea heat and freshwater fluxes as well as hydrographic observations of temperature and salinity (DeVries and Primeau 2011; DeVries 2014). In contrast, the one-dimensional abyssal recipes' inversion of Munk (1966) suggested a value for the vertical diffusivity of $10^{-4}\,m^2\,s^{-1}$, which is an order of magnitude too high for the upper ocean but in agreement with the best present estimate for the deep ocean. Because the vertical diffusivity was a prescribed parameter in our inverse model, it is difficult to tell if the observational constraints provide evidence for the higher deep-ocean value. This deserves further investigation.

Acknowledgments. Eric Deleersnijder is an honorary research associate with the Belgian Fund for Scientific Research. François Primeau is indebted to the Université catholique de Louvain and Delft University of Technology for their financial support. François Primeau also acknowledges support from the National Science Foundation Award OCE 1436922. We are thankful to the reviewers and the editor for the many constructive comments that helped us to improve the paper.

REFERENCES

Antonov, J. I., and Coauthors, 2010: *Salinity*. Vol. 2, *World Ocean Atlas 2009*, NOAA Atlas NESDIS 69, 184 pp.

Bolin, B., and H. Rodhe, 1973: A note on the concepts of age distribution and transit time in natural reservoirs. *Tellus*, **25**, 58–62, doi:10.3402/tellusa.v25i1.9644.

Böning, C. W., and M. D. Cox, 1988: Particle dispersion and mixing of conservative properties in an eddy-resolving model. *J. Phys. Oceanogr.*, **18**, 320–338, doi:10.1175/1520-0485(1988)018<0320:PDAMOC>2.0.CO;2.

Bower, A. S., M. S. Lozier, S. F. Gary, and C. W. Böning, 2009: Interior pathways of the North Atlantic meridional overturning circulation. *Nature*, **459**, 243–247, doi:10.1038/nature07979.

——, ——, and ——, 2011: Export of Labrador Sea Water from the subpolar North Atlantic: A Lagrangian perspective. *Deep-Sea Res. II*, **58**, 1798–1818, doi:10.1016/j.dsr2.2010.10.060.

Broecker, W. S., 1991: The great ocean conveyor. *Oceanography*, **4**, 79–89, doi:10.5670/oceanog.1991.07.

de Boyer Montégut, C., G. Madec, A. S. Fischer, A. Lazar, and D. Iudicone, 2004: Mixed layer depth over the global ocean: An examination of profile data and a profile-based climatology. *J. Geophys. Res.*, **109**, C12003, doi:10.1029/2004JC002378.

Deleersnijder, E., J.-M. Campin, and E. J. M. Delhez, 2001: The concept of age in marine modelling: I. Theory and preliminary model results. *J. Mar. Syst.*, **28**, 229–267, doi:10.1016/S0924-7963(01)00026-4.

Delhez, E. J. M., and E. Deleersnijder, 2002: The concept of age in marine modelling: II. Concentration distribution function in the English Channel and the North Sea. *J. Mar. Syst.*, **31**, 279–297, doi:10.1016/S0924-7963(01)00066-5.

——, A. W. Heemink, and E. Deleersnijder, 2004: Residence time in a semi-enclosed domain from the solution of an adjoint problem. *Estuarine Coastal Shelf Sci.*, **61**, 691–702, doi:10.1016/j.ecss.2004.07.013.

DeVries, T., 2014: The oceanic anthropogenic CO_2 sink: Storage, air-sea fluxes, and transports over the industrial era. *Global Biogeochem. Cycles*, **28**, 631–647, doi:10.1002/2013GB004739.

——, and F. Primeau, 2011: Dynamically and observationally constrained estimates of water-mass distributions and ages in the global ocean. *J. Phys. Oceanogr.*, **41**, 2381–2401, doi:10.1175/JPO-D-10-05011.1.

Doos, K., 1995: Interocean exchange of water masses. *J. Geophys. Res.*, **100**, 13 499–13 514, doi:10.1029/95JC00337.

England, M. H., 1995: The age of water and ventilation timescales in a global ocean model. *J. Phys. Oceanogr.*, **25**, 2756–2777, doi:10.1175/1520-0485(1995)025<2756:TAOWAV>2.0.CO;2.

Fine, A. R., 2011: Observations of CFCs and SF_6 as ocean tracers. *Annu. Rev. Mar. Sci.*, **3**, 173–195, doi:10.1146/annurev.marine.010908.163933.

Fujio, S., and N. Imasato, 1991: Diagnostic calculation for circulation and water mass movement in the deep Pacific. *J. Geophys. Res.*, **96**, 759–774, doi:10.1029/90JC02130.

——, T. Kadowaki, and N. Imasato, 1992: World ocean circulation diagnostically derived from hydrographic and wind stress fields: 2. The water movement. *J. Geophys. Res.*, **97**, 14 439–14 452, doi:10.1029/92JC01227.

Furey, H. H., A. S. Bower, and P. L. Richardson, 2001: Warm water pathways in the northeastern North Atlantic ACCE RAFOS float data report November 1996 - November 1999. Woods Hole Oceanographic Institution Tech. Rep. WHOI-2001-17, 154 pp., doi:10.1575/1912/35.

Gardiner, C. W., 1985: *Handbook of Stochastic Models*. 2nd ed. Springer, 442 pp.

Gary, S. F., M. S. Lozier, C. W. Böning, and A. Biastoch, 2011: Deciphering the pathways for the deep limb of the meridional overturning circulation. *Deep-Sea Res. II*, **58**, 1781–1797, doi:10.1016/j.dsr2.2010.10.059.

Getzlaff, K., C. W. Böning, and J. Dengg, 2006: Lagrangian perspectives of deep water export Atlantic from the subpolar North Atlantic. *Geophys. Res. Lett.*, **33**, L21S08, doi:10.1029/2006GL026470.

Gräwe, U., E. Deleersnijder, S. H. A. M. Shah, and A. W. Heemink, 2012: Why the Euler-scheme in particle-tracking is not enough: The shallow sea test case. *Ocean Dyn.*, **62**, 501–514, doi:10.1007/s10236-012-0523-y.

Haine, T. W. N., and T. M. Hall, 2002: A generalized transport theory: Water-mass composition and age. *J. Phys. Oceanogr.*, **32**, 1932–1946, doi:10.1175/1520-0485(2002)032<1932:AGTTWM>2.0.CO;2.

Hall, T. M., D. W. Waugh, T. W. N. Haine, P. E. Robbins, and S. Khatiwala, 2004: Estimates of anthropogenic carbon in the Indian Ocean with allowance for mixing and time-varying air-sea CO_2 disequilibrium. *Global Biogeochem. Cycles*, **18**, GB1031, doi:10.1029/2003GB002120.

Holzer, M., and T. M. Hall, 2000: Transit-time and tracer-age distributions in geophysical flows. *J. Atmos. Sci.*, **57**, 3539–3558, doi:10.1175/1520-0469(2000)057<3539:TTATAD>2.0.CO;2.

——, and F. W. Primeau, 2006: The diffusive ocean conveyor. *Geophys. Res. Lett.*, **33**, L14618, doi:10.10292006GL026232.

——, and ——, 2008: The path-density distribution of oceanic surface-to-surface transport. *J. Geophys. Res.*, **113**, C01018, doi:10.1029/2006JC003976.

Jazwinski, A. H., 1970: *Stochastic Processes and Filtering Theory*. Academic Press, 376 pp.

Kloeden, P. E., and E. Platen, 1992: *Numerical Solutions of Stochastic Differential Equations*. Stochastic Modelling and Applied Probability Series, Vol. 23, Springer-Verlag, 636 pp.

Large, W. G., J. C. McWilliams, and S. C. Doney, 1994: Oceanic vertical mixing: A review and a model with a nonlocal boundary layer parameterization. *Rev. Geophys.*, **32**, 363–403, doi:10.1029/94RG01872.

Locarnini, R. A., A. V. Mishonov, J. I. Antonov, T. P. Boyer, H. E. Garcia, O. K. Baranova, M. M. Zweng, and D. R. Johnson, 2010: *Temperature*. Vol. 1, *World Ocean Atlas 2009*, NOAA Atlas NESDIS 68, 184 pp.

Lozier, M. S., S. F. Gary, and A. S. Bower, 2012: Simulated pathways of the overflow waters in the North Atlantic: Subpolar to subtropical export. *Deep-Sea Res. II*, **85**, 147–153, doi:10.1016/j.dsr2.2012.07.037.

Mouchet, A., E. Deleersnijder, and F. Primeau, 2012: The leaky funnel model revisited. *Tellus*, **64A**, 19 131, doi:10.3402/tellusa.v64i0.19131.

Munk, W., 1966: Abyssal recipes. *Deep-Sea Res. Oceanogr. Abstr.*, **13**, 707–730, doi:10.1016/0011-7471(66)90602-4.

Peacock, S., and M. Maltrud, 2006: Transit-time distributions in a global ocean model. *J. Phys. Oceanogr.*, **36**, 474–495, doi:10.1175/JPO2860.1.

Primeau, F. W., 2005: Characterizing transport between the surface mixed layer and the ocean interior with a forward and adjoint global ocean transport model. *J. Phys. Oceanogr.*, **35**, 545–564, doi:10.1175/JPO2699.1.

——, and M. Holzer, 2006: The ocean's memory of the atmosphere: residence-time and ventilation-rate distributions of water masses. *J. Phys. Oceanogr.*, **36**, 1439–1456, doi:10.1175/JPO2919.1.

Redi, M. H., 1982: Oceanic isopycnal mixing by coordinate rotation. *J. Phys. Oceanogr.*, **12**, 1154–1158, doi:10.1175/1520-0485(1982)012<1154:OIMBCR>2.0.CO;2.

Richardson, P. L., 2008: On the history of meridional overturning circulation schematic diagrams. *Prog. Oceanogr.*, **76**, 466–486, doi:10.1016/j.pocean.2008.01.005.

Shah, S. H. A. M., A. W. Heemink, and E. Deleersnijder, 2011: Assessing Lagrangian schemes for simulating diffusion on non-flat isopycnal surfaces. *Ocean Modell.*, **39**, 351–361, doi:10.1016/j.ocemod.2011.05.008.

——, ——, U. Gräwe, and E. Deleersnijder, 2013: Adaptive time stepping algorithm for Lagrangian transport models: Theory and idealised test cases. *Ocean Modell.*, **68**, 9–21, doi:10.1016/j.ocemod.2013.04.001.

Solomon, H., 1971: On the representation of isentropic mixing in ocean circulation models. *J. Phys. Oceanogr.*, **1**, 233–234, doi:10.1175/1520-0485(1971)001<0233:OTROIM>2.0.CO;2.

Spivakovskaya, D., A. W. Heemink, G. N. Milstein, and J. G. M. Schoenmakers, 2005: Simulation of the transport particles in coastal waters using forward and reverse time diffusion. *Adv. Water Resour.*, **28**, 927–938, doi:10.1016/j.advwatres.2005.03.005.

——, ——, and E. Deleersnijder, 2007a: The backward Îto method for the Lagrangian simulation of transport processes with large space variations of the diffusivity. *Ocean Sci.*, **3**, 525–535, doi:10.5194/os-3-525-2007.

——, ——, and ——, 2007b: Lagrangian modelling of multi-dimensional advection-diffusion with space-varying diffusivities: theory and idealized test cases. *Ocean Dyn.*, **57**, 189–203, doi:10.1007/s10236-007-0102-9.

Stommel, H., 1958: The abyssal circulation. *Deep-Sea Res.*, **5**, 80–82, doi:10.1016/S0146-6291(58)80014-4.

Talley, L. D., 2013: Closure of the global overturning circulation through the Indian, Pacific, and Southern Oceans: Schematics and transports. *Oceanography*, **26**, 80–97, doi:10.5670/oceanog.2013.07.

Visser, A. W., 2008: Lagrangian modelling of plankton motion: From deceptively simple random walks to Fokker–Planck and back again. *J. Mar. Syst.*, **70**, 287–299, doi:10.1016/j.jmarsys.2006.07.007.

Waterhouse, A. F., and Coauthors, 2014: Global patterns of diapycnal mixing from measurements of the turbulent dissipation rate. *J. Phys. Oceanogr.*, **44**, 1854–1872, doi:10.1175/JPO-D-13-0104.1.